Available online at www.sciencedirect.com
SCIENCE DIRECT
NDT&E International 39 (2006) 96–105
NDT&E international
www.elsevier.com/locate/ndteint

Lamb wave characterization by differential reassignment and non-linear anisotropic diffusion

Oliver Kotte[a], Marc Niethammer[b], Laurence J. Jacobs[a,c,*]

[a]School of Civil and Environmental Engineering, Georgia Institute of Technology, Atlanta, GA 30332-0355, USA
[b]School of Electrical and Computer Engineering, Georgia Institute of Technology, Atlanta, GA 30332-0250, USA
[c]G.W. Woodruff School of Mechanical Engineering, Georgia Institute of Technology, Atlanta, GA 30332-0405, USA

Received 17 June 2005; revised 26 July 2005; accepted 12 August 2005
Available online 7 October 2005

Abstract

This research develops an algorithm which provides excellent localization of Lamb wave dispersion curves while eliminating spurious components. This result is achieved by combining a differential reassignment procedure with non-linear anisotropic diffusion. This study examines the reassignment and diffusion components individually, before developing a combined algorithm. This combined algorithm is then applied to experimentally measured Lamb waves to develop an image of the dispersion curves of a plate with excellent clarity and definition. These dispersion curves are then used to increase the accuracy of a previously developed procedure to locate a notch.

Keywords: Guided waves; Non-linear image smoothing

1. Introduction

Defects in plate-like structures can be located and characterized using the dispersion curves of guided Lamb waves. Previous research by Hurlebaus et al. [1] and Benz et al. [2] has shown that a combination of laser ultrasonics with a time-frequency representation (TFR) can locate a notch in a plate. Notch detection in these procedures relies on the TFR's ability to resolve the individual Lamb modes of the plate, and to localize the energy of the experimentally generated dispersion curves. The specific TFR used in these studies is the reassigned spectrogram [3]; this 'conventional' reassignment method [4] localizes the energy of a spectrogram by direct computation of reassignment coordinates (the corresponding centers of gravity).

Chassande-Mottin et al. [5] present an alternative formulation of this reassignment method, called 'differential' reassignment. Here, the reassignment coordinates are not computed directly, but are inferred through a vector field v, i.e. 'time-frequency particles' travel along the trajectories prescribed by v which can be interpreted as a velocity field for the particles. While conventional and differential reassignment procedures are complementary descriptions, the differential reassignment algorithm combines easily with powerful partial differential equation (PDE) based image processing algorithms. Of particular interest in this paper is non-linear anisotropic diffusion that may be designed to smooth along edges (or ridges), but not across them, thus encouraging intra-region smoothing, while inhibiting inter-region smoothing. Weickert [6] provides a survey of anisotropic diffusion algorithms, and note that this paper uses the Perona-Malik filter [7].

The objective of this research is to enhance previous approaches [3] that characterized experimentally measured Lamb wave signals with a TFR (the reassigned spectrogram). Specifically, the current study combines a 'modified' differential reassignment procedure with non-linear anisotropic diffusion to develop an algorithm that provides excellent localization of Lamb wave dispersion curves, while eliminating spurious components.

This paper first considers differential reassignment and anisotropic diffusion individually. The modified differential reassignment technique developed in this research

* Corresponding author. Address: School of Civil and Environmental Engineering, Georgia Institute of Technology, Atlanta, GA 30332-0355, USA. Tel.: +1 404 894 2771; fax: +1 404 894 2278.
E-mail address: laurence.jacobs@ce.gatech.edu (L.J. Jacobs).

0963-8695/$ - see front matter © 2005 Elsevier Ltd. All rights reserved.
doi:10.1016/j.ndteint.2005.08.001

reparameterizes (in time) the particle trajectories given by differential reassignment [5] to attenuate the reassignment flow along ridges. Note that while a conventionally reassigned spectrogram is computed with a combination of short-time Fourier transforms of suitable windows, the proposed modified differential reassignment method works only in the time-frequency domain (regarded as a two-dimensional image). While working only in the time-frequency domain may at first seem limiting, in reality, it allows for the incorporation of image processing techniques—the desired dispersion curves can now be viewed (and visually improved) in the time-frequency domain. The modified differential reassignment procedure is combined with anisotropic diffusion for smoothing and noise suppression. This combined algorithm is then applied to experimentally measured Lamb waves to develop an image of the dispersion curves of a plate with excellent clarity and definition. These dispersion curves are then applied to a previously developed procedure [2] to locate a notch with increased accuracy.

2. Algorithm development

2.1. Conventional and differential reassignment

The Fourier transform of a transient (time-domain) signal cannot satisfactorily describe non-stationary time signals (i.e. signals with time-varying frequency content). To remedy this deficiency, a large number of TFRs have been developed that are capable of analyzing non-stationary signals; spectrograms (and many other TFRs) are subsumed in the general framework of Cohen's class [8]. The short-time Fourier transform (STFT), is based on the Fourier transform and is defined as

$$F(t,\omega) = \frac{1}{2\pi}\int_{-\infty}^{\infty} \mathrm{e}^{-\mathrm{i}\omega\tau} s(\tau) h(\tau - t)\mathrm{d}\tau, \tag{1}$$

where $h(t)$ is a window function, t is time, and ω is angular frequency. Instead of considering a transform of the entire time-domain signal, $s(t)$, at once, the signal is chopped into a series of small overlapping pieces, and each of these pieces is windowed and then individually Fourier transformed. Its energy density spectrum

$$E_{\mathrm{d}}(t,\omega) = |F(t,\omega)|^2 \tag{2}$$

is called a spectrogram. The spectrogram (and other TFRs) suffers from the Heisenberg uncertainty principle, making it impossible to simultaneously have perfect resolution in both time and frequency [8].

In conventional reassignment, energy is moved from its original point of computation to a center of gravity, thus localizing the information of the spectrogram. Note that reassignment is not only restricted to spectrograms, but can be applied to any time-frequency shift invariant distribution of Cohen's class [8]. Auger and Flandrin [4] show that the reassigned coordinates $\hat{t}$ and $\hat{\omega}$ for the spectrogram can be calculated by

$$\hat{t} = t - \Re\left(\frac{F_{\mathrm{Th}}(t,\omega)F_{\mathrm{h}}^*(t,\omega)}{|F_{\mathrm{h}}(t,\omega)|^2}\right) \tag{3}$$

and

$$\hat{\omega} = \omega - \Im\left(\frac{F_{\mathrm{Dh}}(t,\omega)F_{\mathrm{h}}^*(t,\omega)}{|F_{\mathrm{h}}(t,\omega)|^2}\right) \tag{4}$$

for the STFT, where $F_{\mathrm{h}}(t,\omega)$ is the STFT of the signal using a normalized window function $h(t)$; $F_{\mathrm{Th}}(t,\omega)$ and $F_{\mathrm{Dh}}(t,\omega)$ are the STFTs with t times $h(t)$ and $(\mathrm{d}h(t)/\mathrm{d}t)$ as their respective window functions; a^* denotes the complex conjugate of a; and $\Re$ and $\Im$ are the real and imaginary portions, respectively.

In other words, the conventional reassignment algorithm relocates the energy from each time-frequency point with coordinates $(t,\ \omega)$, to a new reassigned location $(\hat{t}(t,\omega),\hat{\omega}(t,\omega))$. This relocation can be expressed by the displacement vector field

$$\mathbf{r}(t,\omega) = \begin{pmatrix} \hat{t}(t,\omega) - t \\ \hat{\omega}(t,\omega) - \omega \end{pmatrix} \tag{5}$$

defined by Eqs. (3) and (4).

Note that if reassignment moves the energy from several (un-reassigned) time-frequency particles to the same (reassigned) time-frequency point, then their individual values will be summed, thus conserving energy. Calculating the reassignment of a spectrogram produces a much more distinct time-frequency resolution when compared to a non-reassigned spectrogram, and has shown to be highly effective when applied to experimentally measured multi-mode, dispersive Lamb wave signals [9].

Conventional reassignment relocates (energy from) time-frequency particles away from their original, un-reassigned location to their center of gravity. This action can be expressed as a displacement vector field (Eq. (5)). In contrast, differential reassignment uses a velocity vector field to describe the motion of time-frequency particles. First, let the STFT of a signal be denoted by $F(t,\ \omega)$. Then, by using the complex variable $z = \omega + \mathrm{i}t$ and its complex conjugate z^*, the STFT $F(t,\omega)$ can be rewritten as Bargmann factorization

$$F(t,\omega) = \mathscr{F}(z,z^*)\mathrm{e}^{(-|z|^2/4)}. \tag{6}$$

Based on this factorization, Chassande-Mottin et al. [5] deduce that

$$\mathbf{v}(t,\omega) = \nabla \log|F| - 2\begin{pmatrix} \Im\{\partial_{z^*}\log\mathscr{F}\} \\ \Re\{\partial_{z^*}\log\mathscr{F}\} \end{pmatrix} \tag{7}$$

is the desired velocity field, holding over the set $\Re^2\backslash\{(t,\omega)|F(t,\omega) = 0\}$, i.e. it holds everywhere except

at the locations, where the STFT is exactly zero. An interpretation of this result is that given Eq. (6)—the Bargmann factorization of an STFT—its reassignment vector field can be decomposed into two terms. The first term is the gradient of the scalar potential log $|F|$, and the second term is a measure of the non-analyticity of $\mathcal{F}$.

The use of a Gaussian window of unit variance (whose isocontours are circles in a Wigner representation) leads to the Cauchy equations $\partial_{z^*}\mathcal{F} = 0$, and thus

$$\mathbf{v}(t,\omega) = \nabla \log |F|. \tag{8}$$

The reassignment vector field is then identical to the gradient of the scalar potential—log $|F|$ for this case. As a result, the reassignment vectors indicate the direction of steepest ascend of the STFT modulus. The case of a different window (not a Gaussian window of unit variance) is described in [10].

Eq. (7) is a link between the reassignment vector field of Eq. (5) and a scalar potential log $|F|$—the reassignment vector field is the velocity field that controls the motion of each time-frequency contribution $|F(t,\omega)|^2$ considered as a particle, with (t,ω) as its starting (un-reassigned) position. In the unit variance Gaussian case, each particle converges to some maximum of log $|F|$, thus localizing diffuse information by forming peaks and ridges.

2.2. Modified differential reassignment

This research develops a modified differential reassignment algorithm for spectrogram reassignment by using Eq. (8) in a different way. Chassande-Mottin et al. [5] derived Eq. (8) based on the STFT; their variable, F, denotes the complex-valued STFT. This research uses the idea of a logarithmic scalar potential to manipulate images. The square of the STFT magnitude, denoted $|F|$ in Eq. (8) becomes the abstract, two-dimensional scalar field, I (a positive intensity image). In what follows, make the identifications $t \mapsto x$, $\omega \mapsto y$ to facilitate a more standard image processing notation (and not a notation that is directly tied to the current application of differential reassignment). Finally, note that Eq. (8) is valid if the distance between image cells in both dimensions are equal—for convenience, take $\Delta x = \Delta y = 1$. Scaling terms are needed if unequal cell distances are used.

To combine PDE-based image processing algorithms with differential reassignment it is convenient to write the Lagrangian particle evolution equation [5]

$$\boldsymbol{x}_\tau = \boldsymbol{v} \tag{9}$$

where x denotes particle position, τ denotes time, and every particle carries its associated (mass) I in its Eulerian (cell-centered) form which directly describes the evolution of I. (Note that subscripts denote partial derivatives.) The PDE which describes the movement of energy particles is then based on the transport equation

$$I_\tau + v^x I_x + v^y I_y = 0, \tag{10}$$

where the left hand side is simply the material derivative of $\boldsymbol{I}$ given the velocity field $\boldsymbol{v}$, and noting

$$v = \begin{pmatrix} v^x \\ v^y \end{pmatrix} \tag{11}$$

The particle velocity v is given by the reassignment vector of Eq. (8). Plugging Eq. (8) into Eq. (10) (noting that the initial image, I^0, must be non-negative, which is true for all spectrograms) and recalling that $I^0 \equiv |F|^2$ yields

$$I_\tau + (\log I^0)_x I_x + (\log I^0)_y I_y = 0 \tag{12}$$

which describes the numerical reassignment flow. Note that the velocity field $\boldsymbol{v}$ is static and determined by the initial image I^0 only.

The modified differential reassignment algorithm follows the differential reassignment vector field (Eq. (8)), and thus guarantees that energy is moved along differential reassignment trajectories; it works on the well-established mathematical foundation provided by differential reassignment theory.

Scaling of $\boldsymbol{v}$ only reparameterizes the particle trajectories in time. This is expressed by

$$I_\tau + \Theta v^x I_x + \Theta v^y I_y = 0, \tag{13}$$

where $\Theta = \Theta(x,y)$ is a constant scalar field; Θ is a design parameter which introduces a degree of freedom that is used to manipulate the velocity of energy travel along the differential reassignment trajectories. As a result, differential reassignment now occurs with the new velocities $\bar{v}^x = \Theta v^x$ and $\bar{v}^y = \Theta v^y$.

Eq. (13) may be solved numerically by dimensional splitting and the donor-cell upwind method for advection [11]. This scheme ensures that no energy is created or destroyed—the resulting algorithm is fully conservative.

Good results have been obtained with the design parameter

$$\Theta(x,y) = \mathrm{e}^{-(I^0(x,y)/\max(I^0(\cdot,\cdot)))}. \tag{14}$$

This choice uses an exponential function to ensure that Θ helps to further attenuate reassignment flow in high energy regions, namely along ridges. Discussion of Θ selection, step size, and stability is presented in [10]. An example of the modified differential reassignment algorithm operating on a synthetic image is shown in Appendix A.

2.3. Non-linear anisotropic diffusion

Non-linear anisotropic diffusion [6,7] encourages intra-region smoothing and inhibits inter-region smoothing, thus preserving edges. (Note that isotropic diffusion does not preserve edges.)

This paper is concerned with non-linear anisotropic diffusion of the form

$$I(x,y,\tau)_\tau = \nabla\cdot[c(x,y,\tau)\nabla I(x,y,\tau)]. \tag{15}$$

In this research, $I(x, y, \tau)$ is the squared STFT modulus, the spectrogram. The diffusion function $c(x, y, \tau)$ is selected such that

$$c(x,y,\tau) = f(|\nabla I(x,y,\tau)|). \tag{16}$$

This allows for locally adaptive diffusion strengths—edges are selectively smoothed or enhanced. Although any monotonically decreasing continuous function of ∇I would suffice as a diffusion function, the two functions

$$c_1(x,y,\tau) = \mathrm{e}^{-(|\nabla I(x,y,\tau)|/\kappa)^2} \tag{17}$$

$$c_2(x,y,\tau) = \frac{1}{1+\left(\frac{|\nabla I(x,y,\tau)|}{\kappa}\right)^{1+\alpha}}, \alpha > 0 \tag{18}$$

are proposed by [7] and are shown in Fig. 1(a).

The parameter κ is referred to as the diffusion constant or the flow constant. Obviously, the behavior of the diffusion process depends on κ. To clarify the effect of κ (and the diffusion function) on the diffusion process, it is helpful to define the flow function

$$\Phi(x,y,\tau) = c(x,y,\tau)\nabla I(x,y,\tau). \tag{19}$$

Eq. (15) can then be rewritten as

$$I(x,y,\tau)_\tau = \nabla\Phi(x,y,\tau). \tag{20}$$

The flow functions, Φ_1 and Φ_2, corresponding to the diffusion functions, c_1 and c_2, are plotted in Fig. 1(b).

Notice that flow increases with the gradient to the point where $|\nabla I(x,y,\tau)| \simeq \kappa$, then decreases to zero. This behavior implies that the diffusion process maintains homogeneous regions, where $|\nabla I(x,y,\tau)| \ll \kappa$, since little flow is generated. Similarly, edges are preserved because the flow is small in regions, where $|\nabla I(x,y,\tau)| \gg \kappa$.

The greatest flow is produced when the image gradient magnitude is close to the value of κ—by choosing κ to correspond to gradient magnitudes produced by noise, the diffusion process can be used to reduce noise in images. Assuming an image contains no discontinuities, object edges can be enhanced by choosing a value of κ slightly less than the gradient magnitude of the edges.

The discrete implementation of non-linear anisotropic diffusion (Eq. (15)) is fairly straightforward and its 2-dimensional form is presented in [10], while a numerical example is shown in Appendix B.

2.4. Combined algorithm—modified differential reassignment superimposed with non-linear anisotropic diffusion

The proposed combined algorithm consists of the carefully weighted contributions of differential reassignment and non-linear anisotropic diffusion. To balance reassignment with diffusion, a weighting factor

$$\beta = \frac{\Delta\tau_{\text{reassignment}}}{\Delta\tau_{\text{diffusion}}} \tag{21}$$

is introduced, reflecting the relation between reassignment and diffusion step sizes. Finding a suitable value for β involves an iterative trial-and-error approach. If the reassignment part is too strong, β has to be increased. If the image is diffused too much, then β has to be reduced.

Image evolution is then expressed by a PDE governing energy movement

$$I_\tau + \Theta(\log I^0)_x I_x + \Theta(\log I^0)_y I_y - \beta[(c_1 I_x)_x + (c_1 I_y)_y] = 0. \tag{22}$$

Θ is selected using Eq. (14) together with the diffusion function c_1 according to Eq. (17) which (together with Eq. (22)) yields

$$I_\tau + \mathrm{e}^{-(I^0/\max(I^0))}(\log I^0)_x I_x + \mathrm{e}^{-(I^0/\max(I^0))}(\log I^0)_y I_y - \beta\left[(\mathrm{e}^{-((1/\kappa)|I_x|)^2} I_x)_x + (\mathrm{e}^{-((1/\kappa)|I_y|)^2} I_y)_y\right] = 0. \tag{23}$$

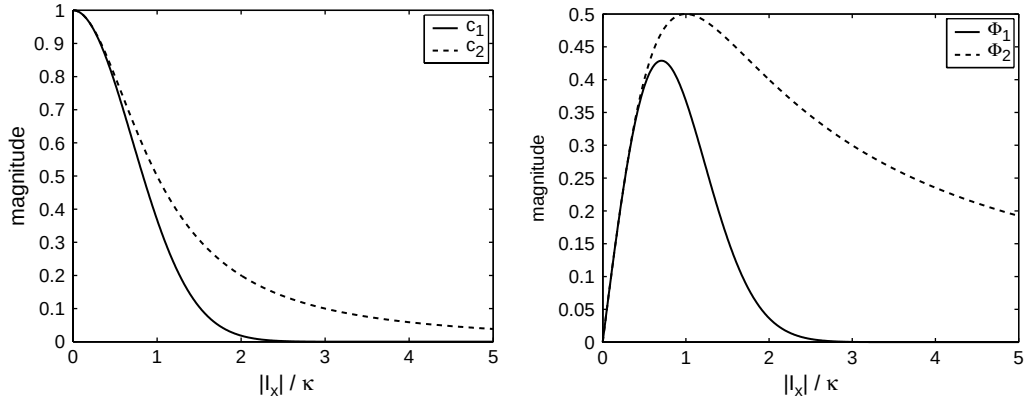

(a) Diffusion functions (b) Flow functions

Fig. 1. Diffusion and flow functions.

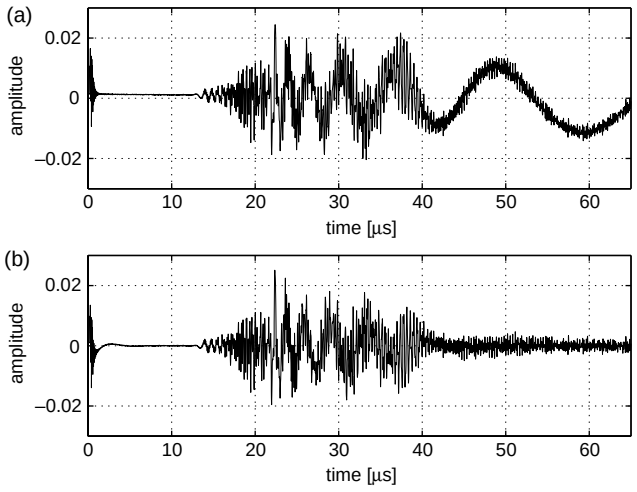

Fig. 2. Time-domain signal before (top) and after (bottom) high-pass filtering.

With the un-reassigned (or conventionally reassigned) spectrogram as the initial condition and Neumann boundary conditions, this PDE fully describes the image evolution of the combined algorithm.

3. Application of the combined algorithm to lamb waves

3.1. Perfect plate results

Consider the application of the combined algorithm to Lamb waves measured in a (perfect, un-notched) polished 3003 aluminum plate with dimensions 305 mm × 610 mm × 0.99 mm. A Q-switched, Nd:YAG pulse laser serves as the ultrasonic source (non-contact, broad frequency bandwidth, point-like) and a dual probe heterodyne interferometer (non-contact, high fidelity, point-like) serves as the detection system (see [1], [2] and [9] for details of the instrumentation and measurements).

A typical time-domain signal is first high-pass filtered with a third order Butterworth filter having a cutoff frequency of 200 kHz, shown in Fig. 2 before and after high-pass filtering. The noise spike at time $t=0$ is due to the electromagnetic discharge of the Nd:YAG source laser, is spurious, and is windowed out of the time-domain signal before processing. The high-pass filtered time-domain signal is used to calculate the un-reassigned spectrogram shown in Fig. 3, which is presented with the theoretical mode solutions—the solid black lines in Fig. 3 and in all future images. Note that the spectrogram (and theoretical mode lines) has been converted to the slowness-frequency domain by normalizing the signal with respect to propagation distance; given a propagation distance d and time t, energy slowness is defined as $sl_e = t/d$. This transformation is linear in time, so it does not impact the image processing.

Conventional reassignment is applied to the same high-pass filtered time-domain signal in Fig. 2 to obtain a reassigned version of the same experimentally measured spectrogram and shown in Fig. 4. Spurious components introduced by the reassignment algorithm are clearly visible; Fig. 5(a) is a zoomed-in view of the slowness-frequency region [3–4.5 MHz, 350–420 sl_e]. Ridges are far from smooth, spurious peaks are visible, and noise is generally present.

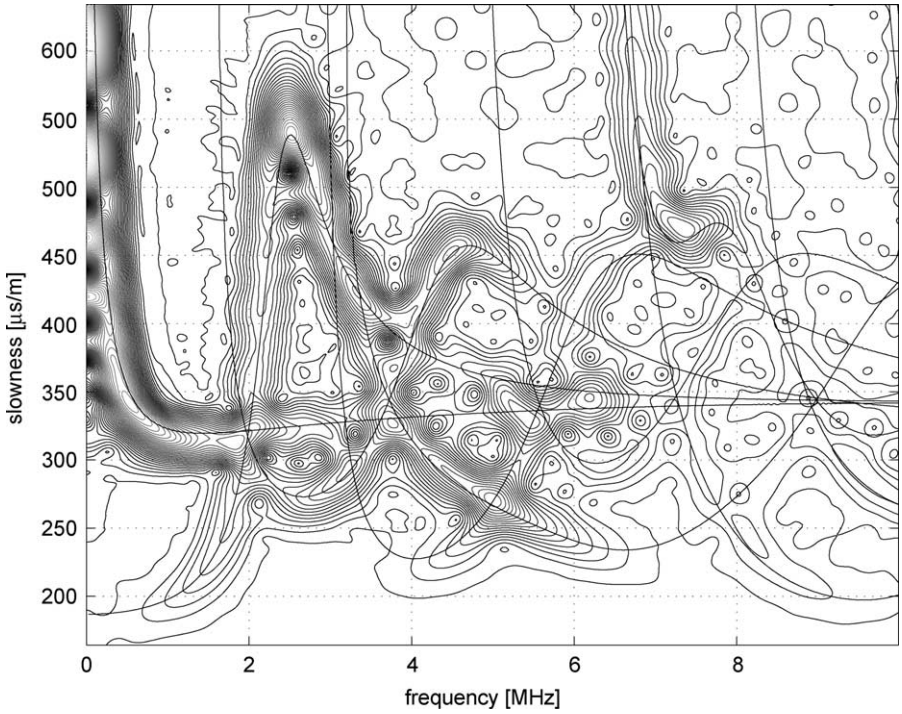

Fig. 3. Un-reassigned spectrogram.

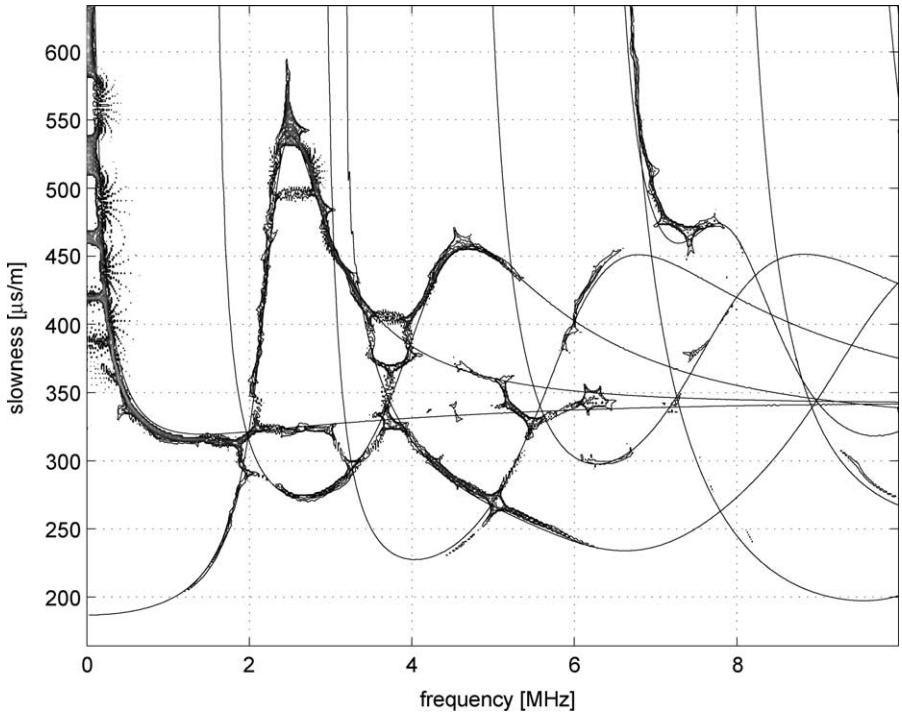

Fig. 4. Conventionally reassigned spectrogram.

The combined algorithm (modified differential reassignment superimposed with anisotropic diffusion) is instead applied to the un-reassigned spectrogram shown in Fig. 3. The free parameters used in the combined algorithm are $\beta = 5\times10^{-4}$, $\kappa = 1.3$, $\Delta\tau = 0.0158$ and 60,000 iterations—Fig. 6 shows the final image. It is clear from Fig. 6 that differential reassignment moves energy towards the theoretical dispersion curves, building up the sharp edges and pressing ridges together. In addition, reassignment movement along the ridges forms peaks and dips. However, the anisotropic diffusion algorithm diffuses energy along these ridges, attenuates undesirable reassignment effects, and forms smooth, localized curves.

A comparison of Figs. 4 and 6 shows that the combined algorithm includes significant energy that corresponds to the theoretical dispersion curves (especially in the higher frequencies) which does not appear in the conventionally reassigned spectrogram—the combined algorithm extracts more information from the same time-domain signal. It is important to note that the combined algorithm dispersion curves are smoother than their conventionally reassigned counterparts. This becomes more obvious when considering the zoomed-in views shown in Fig. 5(a) and (b). The combined algorithm results in smoother ridges, as well as the elimination of both spurious peaks and noise.

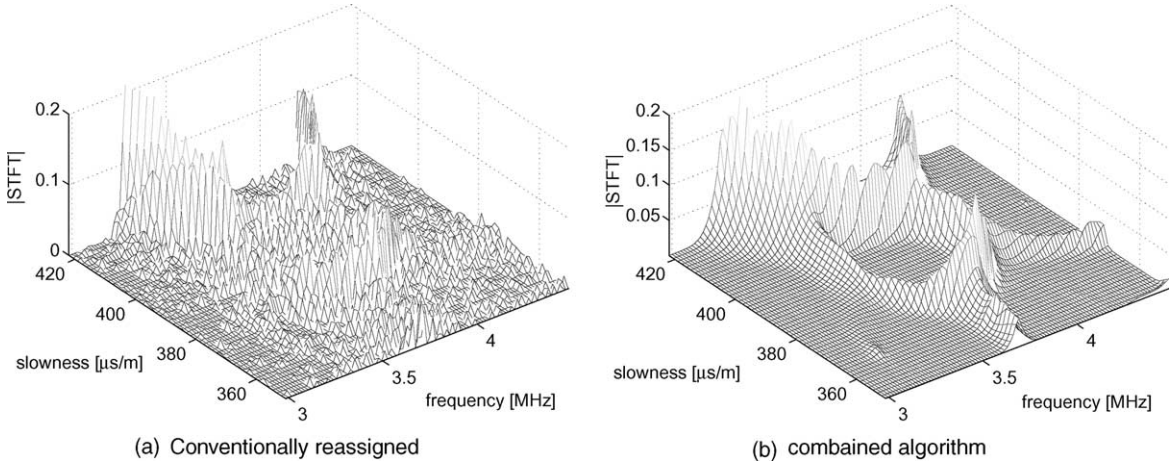

Fig. 5. Comparison of zoomed-in regions of spectrograms.

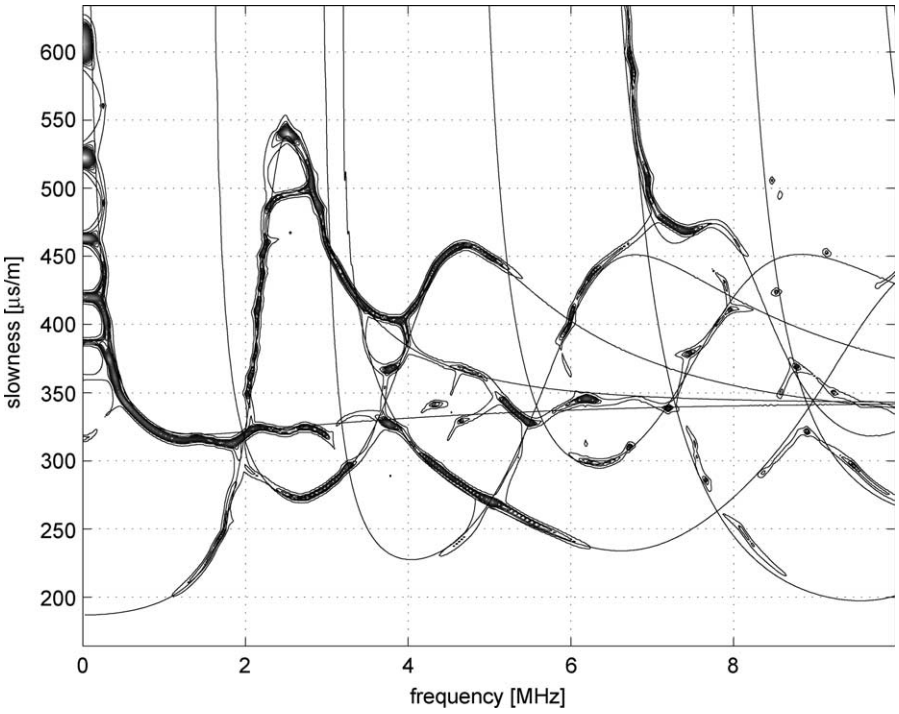

Fig. 6. Combined algorithm image.

Finally, if energy conservation is not an issue, but instead a clear image of the experimentally measured data is desired, then a 'threshold', δ, can be applied to the combined algorithm image. Fig. 7 (free parameters: $\beta = 5 \times 10^{-4}$, $\kappa = 1.3$, $\Delta\tau = 0.0158$ and 60,000 iterations) shows the image obtained when the values below $\delta = 0.004$ in Fig. 6 are set equal to zero, and the values above $\delta = 0.004$ in Fig. 6 are set equal to unity. This yes/no approach (which does not conserve energy) can be used in visualization applications, where a crisper image is more important than energy conservation.

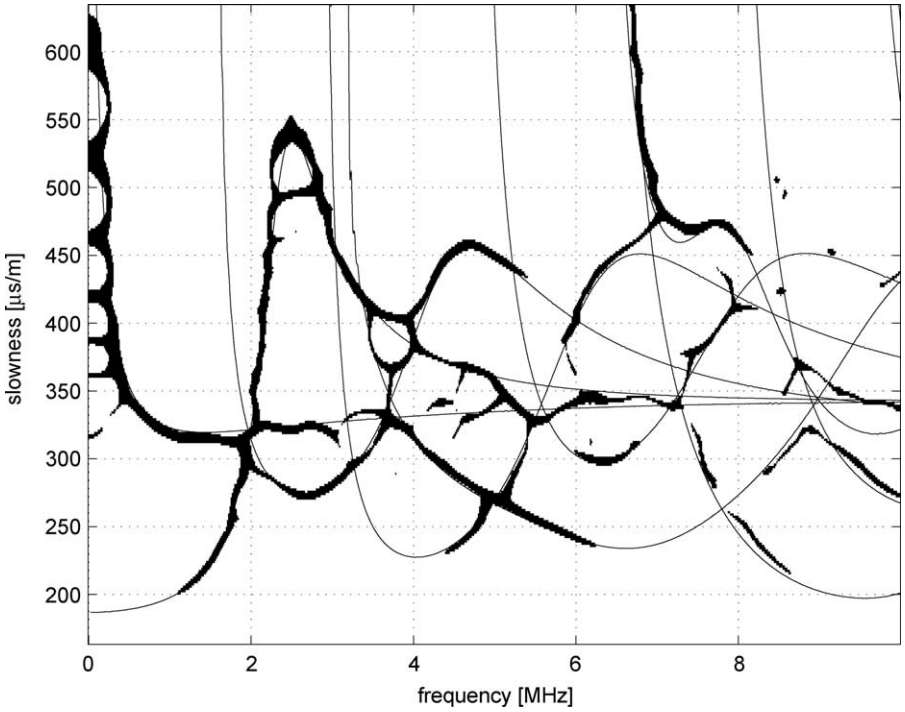

Fig. 7. Combined algorithm image without conserving energy ($\delta = 0.004$).

3.2. Notch localization

Previous research [2] formulated a correlation technique to locate a notch in this same (0.99 mm thick) 3003 aluminum plate using the reflected Lamb wave field. This procedure uses an understanding of the multi-mode, dispersive nature of Lamb waves, and is enhanced by selection of frequency bands that contain significant reflected energy. The results presented in [2] were calculated using conventionally reassigned spectrograms of the perfect and notched plates. Since the combined algorithm developed in the current study provides an increase in spectrogram clarity when compared to the conventionally reassigned algorithm, a final demonstration applies this new combined algorithm to the correlation procedure presented in [2].

In brief, the technique in [2] examines a correlation of the spectrograms measured in a notched plate (known location of this notch is $\Delta d_0' = 29.2$ mm) and in a perfect plate—each calculated with different, assumed propagation distances ($\Delta d_0'$). Reflections (from the notch and any plate edges) will introduce local maxima in the correlation curves at certain propagation distances. These local maxima occur when the reflected modes (within a spectrogram) coincide with the incident modes, which in turn provide a notch (or plate edge) location distance. A ratio of the notched to perfect plate correlations removes the maxima due to plate edges (the edges are present in both notched and plate specimens) and will show maxima only at 'reflecting' features that are present in the notched plate, but not in the perfect plate. The notch is the only such feature in these experiments. An additional procedure limits the correlation region to frequency bandwidths with high reflected energy.

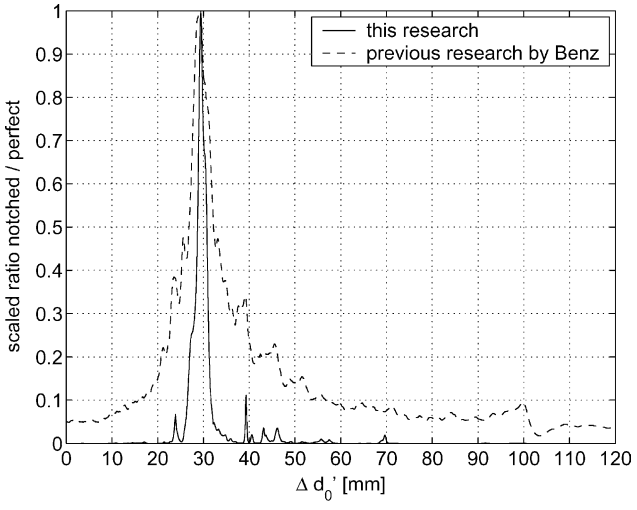

Fig. 8. Ratio curve for the frequency band 330 kHz–2 MHz, with threshold δ.

Fig. 8 shows two ratio curves (ratio of the correlations of the notched to perfect plates), each obtained when limiting the correlation to a frequency band of 330 kHz–2 MHz. One ratio curve is determined with spectrograms calculated using the combined algorithm developed in this research, while the other curve is based on the same conventional reassignment procedure used in [2].

Both algorithms lead to very accurate notch localization—they both contain peaks at the correct notch location distance of $\Delta d_0' = 29.2$ mm to within ± 0.1 mm. However, the ratio curve calculated with the combined algorithm has a peak that is much sharper, and this sharp peak provides a more definitive indication of the notch location. The sharpness of this peak also suggests that the combined algorithm will be more effective in complicated applications (such as the case of two closely spaced reflectors), where multiple correlation peaks could be close to one another.

4. Conclusion

This research establishes the effectiveness of applying advanced image processing techniques to characterize multi-mode, dispersive Lamb waves. This work makes a contribution in bridging the gap between image processing and non-destructive evaluation, by clearly demonstrating the effectiveness of applying image processing techniques to representations of experimentally measured Lamb waves.

Specifically, this research combines a classical signal processing technique (the spectrogram, a time-frequency representation) with edge-preserving smoothing—an image processing technique. In particular, the differential form of time-frequency reassignment is employed to facilitate its combination with powerful PDE-based non-linear anisotropic diffusion, with the goal of image smoothing and noise reduction, while still preserving edge information.

The proposed modified differential reassignment algorithm provides Lamb wave dispersion curves of excellent clarity and definition while suppressing noise. The numerics of the proposed modified differential reassignment algorithm are designed to conserve energy. While quantitative, local, physical conclusions regarding energy distributions across frequencies and over modes are not per se possible with reassignment procedures based on center of mass considerations (it is not clear that assigning energy to centers of gravity results in physically meaningful results), the proposed modified reassignment procedure allows for qualitative measurements of mode energies and successfully reduces noise levels.

This advantage is demonstrated in an application that uses the reflected energy contained in multi-mode, dispersive Lamb waves. By using a correlation procedure developed by [2], the combined algorithm is used to locate a notch in a plate with a high degree of accuracy and confidence.

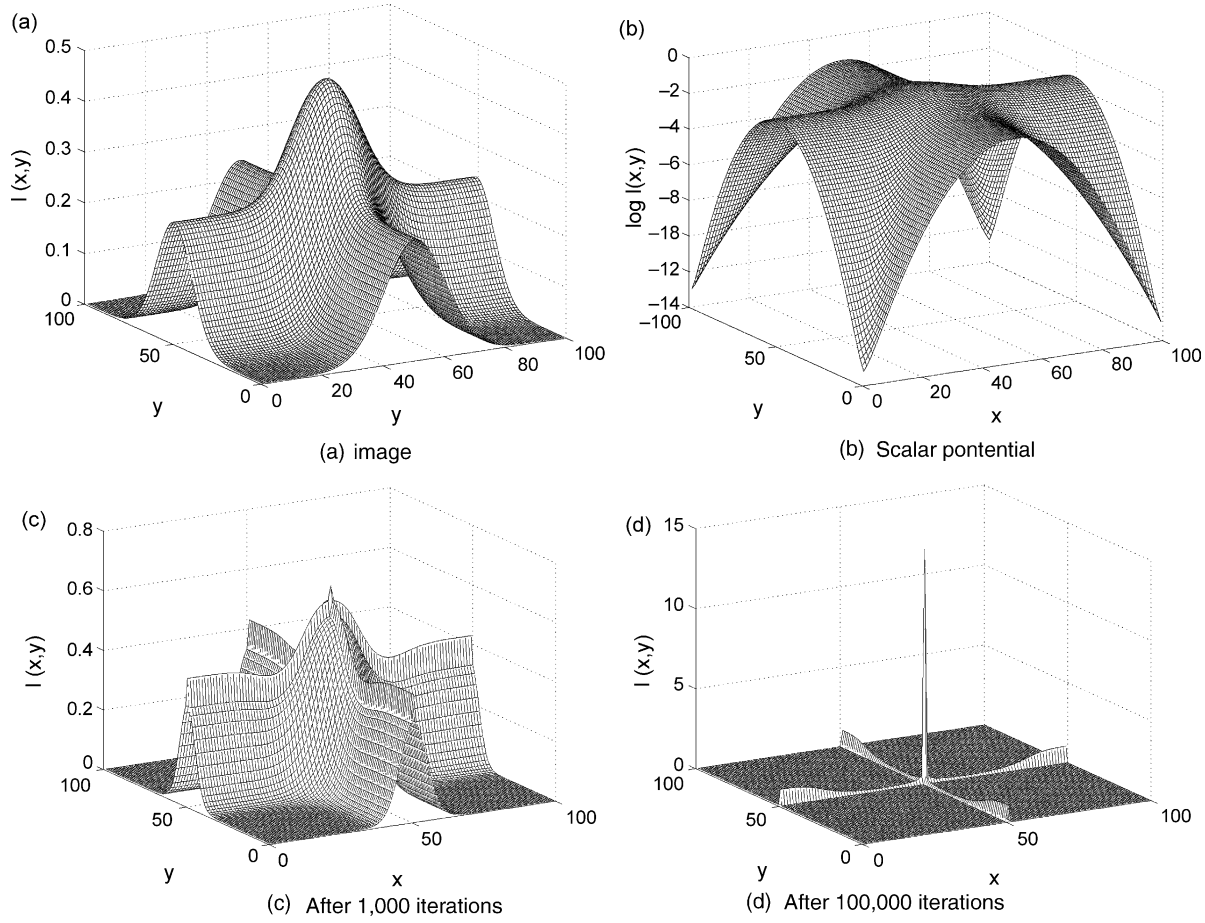

Fig. A1. Differential reassignment example.

Acknowledgements

The Deutscher Akademischer Austausch Dienst (DAAD) provided partial support to Oliver Kotte.

Appendix A. Modified differential reassignment example

Consider a 2-dimensional example using the modified differential reassignment algorithm that uses a quadratic image with a resolution of 100×100 ($\Delta x=\Delta y=1$) cells. The analytic, initial image follows the Gaussian function

$$I(x,y)=\frac{1}{\pi^4\sqrt{\sigma}}e^{-((x-50)^2/2\sigma^2)}+\frac{1}{\pi^4\sqrt{\sigma}}e^{-((y-50)^2/2\sigma^2)} \quad (24)$$

with standard deviation $\sigma=10$—this function is shown in Fig. A.1(a) and (b) shows its scalar potential. This particular image is selected to demonstrate the ability of the proposed

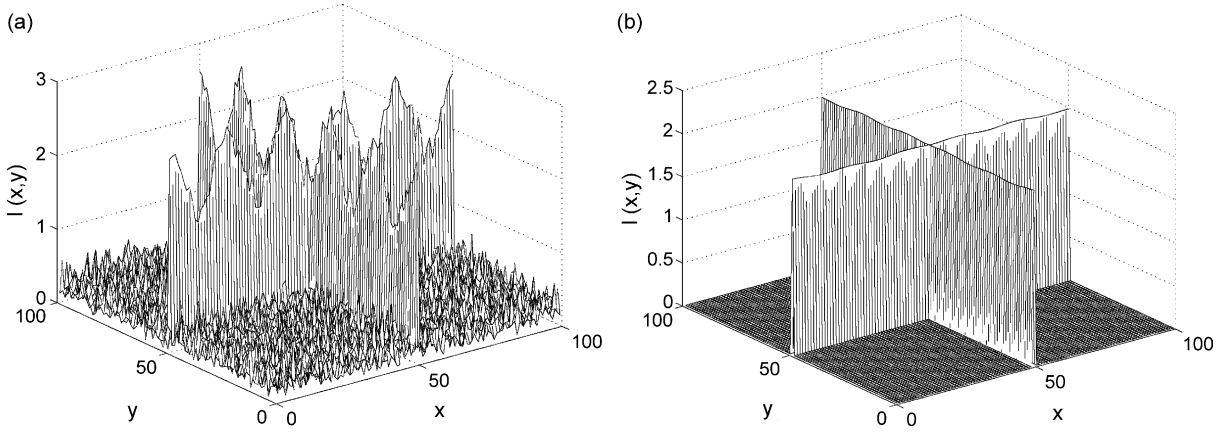

Fig. B1. Non-linear anisotropic diffusion example.

differential reassignment algorithm to provide localization of a ridge and reassignment flow towards this ridge.

The modified differential reassignment algorithm (free parameter $\Delta\tau = 0.0158$) is applied and the evolution is shown after 1000 and 10,000 iterations in Fig. A1(c) and (d). These images show that ridges and ridge intersections are well localized—ridge edges are steep and the 'dip' formation is comparatively weak.

Appendix B. Non-linear anisotropic diffusion example

Consider a 2-dimensional example using the proposed non-linear anisotropic diffusion algorithm that uses an image of 100×100 ($\Delta x = \Delta y = 1$) cells that is zero except for the central horizontal and vertical lines

$$I(x, 50) = 3 + \frac{1}{2}\cos\left(\frac{\pi}{10}x\right)$$
$$I(50, y) = 3 + \frac{1}{2}\cos\left(\frac{\pi}{10}y\right) \quad (25)$$

and contains random noise with a maximum magnitude of one added. The resulting image is shown in Fig. B1(a) and serves as initial image for demonstration purposes. This particular image is selected to demonstrate the ridge preserving nature and noise suppression of anisotropic diffusion.

This example uses $\kappa = 0.5$ and $\Delta\tau = 0.2$ as free parameters, and Fig. B.1(b) shows the result after 200 iterations. The anisotropic diffusion algorithm has excellent performance with regard to three different aspects: (i) noise is diffused; (ii) sharp edges are preserved; and (iii) dips on the ridges are smoothed out. Note that the 'mass' of 2, 738 units is preserved throughout the algorithm.

References

[1] Hurlebaus S, Niethammer M, Jacobs LJ, Valle C. Automated methodology to locate notches with Lamb waves. Acoust Res Lett Online 2001;(4):97–102.
[2] Benz R, Niethammer M, Hurlebaus S, Jacobs LJ. Localization of notches with Lamb waves. J Acoust Soc Am 2003;114(2):677–85.
[3] Niethammer M, Jacobs LJ, Qu J, Jarzynski J. Time-frequency representation of Lamb waves. J Acoust Soc Am 2001;109(5):1841–7.
[4] Auger F, Flandrin P. Improving the readability of time-frequency and timescale representations by the reassignment method. IEEE Trans Signal Process 1995;43(5):1068–89.
[5] Chassande-Mottin E, Daubechies I, Auger F, Flandrin P. Differential reassignment. IEEE Signal Process Lett 1997;4(10):293–4.
[6] Weickert J. In: Lecture notes in computer science. In: Ch. A review of non-linear diffusion filtering, vol. 1252. Heidelberg: Springer-Verlag; 1997. p. 3–28.
[7] Perona P, Malik J. Scale-space and edge detection using anisotropic diffusion. IEEE Trans Pattern Anal Mach Intell 1990;12(7):629–39.
[8] Cohen L. Time-frequency Analysis. Englewood Cliffs, NJ: Prentice Hall; 1995.
[9] Niethammer M, Jacobs LJ, Qu J, Jarzynski J. Time-frequency representation of Lamb waves using the reassigned spectrogram. J Acoust Soc Am 2000;107(5):L19–L24.
[10] O. Kotte. Application of image processing techniques for Lamb wave characterization, Master's thesis, Georgia Institute of Technology; 2004.
[11] LeVeque R. Finite Volume Methods for Hyperbolic Problems. Cambridge, USA: Cambridge University Press; 2002.